Contents lists available at SCCE

Journal of Soft Computing in Civil Engineering

Journal homepage: www.jsoftcivil.com

Using the Artificial Neural Network to Predict the Axial Strength and Strain of Concrete-Filled Plastic Tube

N.A. Abdulla[1*]

1. Assistant Professor, Department of Civil Engineering, College of Engineering, Salahaddin University, Erbil, Republic of Iraq

Corresponding author: *anwzad@yahoo.com*

https://doi.org/10.22115/SCCE.2020.225161.1198

ARTICLE INFO

Article history:
Received: 31 March 2020
Revised: 10 May 2020
Accepted: 28 May 2020

Keywords:
Plastic encasement,
Confined concrete;
Compressive strength;
Strain at ultimate strength;
Artificial neural network.

ABSTRACT

The main purpose of the current study was to formulate an empirical expression for predicting the axial compression capacity and axial strain of concrete-filled plastic tubular specimens (CFPT) using the artificial neural network (ANN). A total of seventy-two experimental test data of CFPT and unconfined concrete were used for training, testing, and validating the ANN models. The ANN axial strength and strain predictions were compared with the experimental data and predictions from several existing strength models for fiber-reinforced polymer (FRP)-confined concrete. Five statistical indices were used to determine the performance of all models considered in the present study. The statistical evaluation showed that the ANN model was more effective and precise than the other models in predicting the compressive strength, with 2.8% AA error, and strain at peak stress, with 6.58% AA error, of concrete-filled plastic tube tested under axial compression load. Similar lower values were obtained for the NRMSE index.

1. Introduction

In the present-days more and more data are becoming available in the literature for the structural performance of concrete-filled plastic tubes (CFPT). The potential of engineering plastics has been harnessed for a few applications in civil engineering including columns and piers [1,2]. CFPT columns are becoming an interesting option for researchers due to its many advantages. It

How to cite this article: Abdulla NA. Using the artificial neural network to predict the axial strength and strain of concrete-filled plastic tube. J Soft Comput Civ Eng 2020;4(2):63–84. https://doi.org/10.22115/scce.2020.225161.1198.

has good structural performance, such as excellent ductility, sufficient load-bearing capacity, large energy absorption capacity, and strong resistance to environmental influences including good resistance to corrosion and chemicals [3]. Generally a material with large stiffness yields a smaller fracturing strain (smaller ductility). The material cost is usually higher when the strength/stiffness of the material is higher. A CFPT element is constructed by pouring concrete into a hollow plastic tubular.

One of the main advantages of CFPT elements is that they combine the material properties of the two components employed in the design and construction of the column. The stiffer concrete core delays local buckling in plastic tubular. In return the tube offers concrete the space to dilate and deform to avoid the usual brittle failure. The plastic tubular assist in the resisting of tensile forces, shear forces, bending moments and eliminates the need for formwork for concrete casting and thus led to a reduction in the labor and material cost and improvement in the efficiency of construction [2] . The use of engineering plastics has been transferred from laboratory research to practical applications. Based on the latest developments in PVC technology, multi-layer uPVC is a new plastic characterized by superior properties such as more toughness and reduced weight. The better function and complexity in tube design is grown out of merely small particles [4]. Experimental tests are time-consuming and alternative techniques have been explored by researchers to determine the strength, using theoretical or empirical approaches [5]. Several expressions have been proposed by researchers to determine the mechanical properties of concrete using soft computing procedures. The objective of the present study was to evaluate the ability of the ANN methods to predict the load-carrying capacity of CFPT relative to the parameters used for experimental test data.

Several studies have reported ANN to be a feasible tool for predicting the compressive strength of concrete. Six input parameters were selected by Noorzaei et al. [6] to set up ANN models for predicting the compressive strength of concrete. A total of 639 different data sets of concrete were used. Two hidden layers were considered and the ANN model with 6-12-6-1 architecture showed the best performance. Using ANN to predict concrete strength was shown to be practical and beneficial. Hakim et al. [7] assembled a total of 368 different data for high-strength concrete (HSC) mix-designs from technical literature and used it to construct, train, and test the adopted ANN models. Eight input parameters were considered including cement, water, coarse aggregate, fine aggregate, silica fume, superplasticizer, fly ash and granulated grated blast furnace slag employed.

The ANN technique was reported to follow a detailed mathematical approach within a heuristic scheme [5]. Raghu et al.[8] developed ANN models to predict the 28-days compressive strength of normal and high strength self-compacting concrete (SCC) as well as high-performance concrete (HPC) with high volume fly ash. In addition to the compressive strengths, the slump flow of SCC was also estimated by the proposed neural network, which was validated by the experimental results. Uysal and Tanyildizi [9] have adopted ANN modeling for predicting the compressive strength of SCC containing mineral additives and polypropylene (PP) fibers after exposure to elevated temperatures. It was found that the empirical model produced a high prediction capability of the loss in compressive strength of SCC. Using ANN as a non-linear statistical data modeling tool, a strong correlation between the micro-structural properties of

cement mortar, obtained from digital image analysis, and the compressive strength was reported [10]. The development of techniques to confine concrete has been the subject of research during the last four decades [11]. In a new approach, Naderpour et al. [12] employed artificial neural networks to predict the compressive strength of FRP confined concrete based on a large number of experimental data. The idealized neural network was employed to generate empirical charts and equations for use in design. The 8-10-6-1 architecture was the best possible architecture. The results illustrate that the relative percentage error (RPE) was 7.02% for the training set and 12.64% for the testing set. uPVC has been shown to be an ample and cost-effective material for encasing concrete [13].

The reliability of axially loaded CFPT columns was assessed [14] in terms of reliability index and a relationship between reliability index and strength reduction factor for columns with and without uPVC tube was proposed. The strength reduction factor mandated by the ACI code was modified for CFPT specimens to account for the uncertainties associated with the design variables. The application of a fuzzy inference system (FIS) to predict the strength of CFPT was investigated [15]. Two models with three inputs, one output, and twenty linguistic rules were constructed. The models proved to be very effective in predicting the ultimate strength of CFPT. From the above review, there is no study on the application of ANN technique to predict compressive strength and strain of CFPT which is the objective of the present study.

2. Research significance

There is no study on the application of ANN technique to predict the compressive strength and strain at ultimate strength of CFPT. The present study focuses on evaluating the ability of the ANN methods to give predictions for load-carrying capacity of CFPT relative to the parameters used for experimental test data.

3. Experimental program

3.1. Materials

For making concrete, 20mm maximum aggregate size river coarse aggregate was mixed with hydraulic cement and well-graded sand in a drum-type laboratory concrete mixer. The aggregate/cement ratio was altered from 3 to 8.5 in increments of 0.5 and twelve concrete batches were used to cast 36 CFPT specimens and their equivalent concrete specimens without the plastic tube. The material details of all the specimens and the fresh concrete test results were summarized in Table 1.

3.2. Plastic tube

The low stiffness plastic tube acts as formwork for fresh concrete and as an encasement for hardened concrete. The low-cost tube was characterized by large elongation at failure, 35%, and therefore it contained the fracture and excessive dilation of concrete. The geometric details of the plastic tube and the yield strength of coupon tested in tension (as per ASTM D638) were summarized in Table 1.

Table 1
Mix details and properties of fresh concrete and uPVC tube.

Specimen	Mix ratio	w/c ratio	a/c ratio	Slump(mm)	t_P (mm)	D_P (mm)	fy(MPa)
CT-A1	1:2:1	0.435	3.0	12	3.8	102	40
CT-A2	1:2:1	0.435	3.0	12	3.8	102	40
CT-A3	1:2:1	0.435	3.0	12	3.8	102	40
CT-B1	1:2:1.5	0.450	3.5	10	3.8	102	40
CT-B2	1:2:1.5	0.450	3.5	10	3.8	102	40
CT-B3	1:2:1.5	0.450	3.5	10	3.8	102	40
CT-C1	1:2:2	0.485	4.0	9.5	3.8	102	40
CT-C2	1:2:2	0.485	4.0	9.5	3.8	102	40
CT-C3	1:2:2	0.485	4.0	9.5	3.8	102	40
CT-D1	1:2:2.5	0.505	4.5	9.5	3.8	102	40
CT-D2	1:2:2.5	0.505	4.5	9.5	3.8	102	40
CT-D3	1:2:2.5	0.505	4.5	9.5	3.8	102	40
CT-E1	1:2:3	0.51	5.0	8	3.8	102	40
CT-E2	1:2:3	0.51	5.0	8	3.8	102	40
CT-E3	1:2:3	0.51	5.0	8	3.8	102	40
CT-F1	1:2:3.5	0.51	5.5	7	3.8	102	40
CT-F2	1:2:3.5	0.51	5.5	7	3.8	102	40
CT-F3	1:2:3.5	0.51	5.5	7	3.8	102	40
CT-G1	1:2:4	0.52	6.0	5	3.8	102	40
CT-G2	1:2:4	0.52	6.0	5	3.8	102	40
CT-G3	1:2:4	0.52	6.0	5	3.8	102	40
CT-H1	1:2:4.5	0.535	6.5	5	3.8	102	40
CT-H2	1:2:4.5	0.535	6.5	5	3.8	102	40
CT-H3	1:2:4.5	0.535	6.5	5	3.8	102	40
CT-I1	1:2:5	0.56	7.0	4	3.8	102	40
CT-I2	1:2:5	0.56	7.0	4	3.8	102	40
CT-I3	1:2:5	0.56	7.0	4	3.8	102	40
CT-J1	1:2:5.5	0.585	7.5	2.5	3.8	102	40
CT-J2	1:2:5.5	0.585	7.5	2.5	3.8	102	40
CT-J3	1:2:5.5	0.585	7.5	2.5	3.8	102	40
CT-K1	1:2:6	0.6	8.0	0.0	3.8	102	40
CT-K2	1:2:6	0.6	8.0	0.0	3.8	102	40
CT-K3	1:2:6	0.6	8.0	0.0	3.8	102	40
CT-L1	1:2:6.5	0.605	8.5	0.0	3.8	102	40
CT-L2	1:2:6.5	0.605	8.5	0.0	3.8	102	40
CT-L3	1:2:6.5	0.605	8.5	0.0	3.8	102	40

3.3. Stress-strain behavior

After 28days curing, the specimens were tested under concentric compression load. The axial deformation was recorded at each load increment using two LVDT. The plastic tube maintained a good pre-yield stiffness and it was comparable with concrete, but the stiffness in the post-yield stage (secant modulus) started to drop faster with the increased concrete dilation but without reaching the fracturing point, Fig. 1. The maximum and minimum strain values for confined concrete specimens tested in this research varied from 0.005 to 0.0112, and the corresponding compressive strength varied from 28.98MPa to 47.31MPa, Table 2. CFPT is an element that meets a special combination of performance and ductility requirements that cannot be achieved using brittle concrete [16]. Large tangential, radial and shear stresses are reported to occur at the interface between aggregate and the matrix as a result of the elastic mismatch between aggregate

and matrix [17]. The bond cracks in concrete join with the matrix cracks resulting in material discontinuity due to the formation of an interconnected network of bond and matrix cracks.

Fig. 1. Deformation of CFPT under load.

4. Soft computing techniques

4.1 Artificial neural network

The structure of ANN models included three layers of neurons; input, hidden, and output. The three layers were linked through connections called weight. Two sets of weights give high flexibility to adapt to the data freely: the input-hidden layer weights ($w_{j,i}$) and the hidden-output layer weights (w_{kj}). The neurons in the input layer receive information from the outside environment and transmit them to the neurons of the hidden layer without performing any calculation. The output of typical multilayer perceptron ANN with a single layer of hidden neurons is expressed by:

$$\hat{y}_K = f_o\left[\sum_{j=1}^{m}\left\{w_{kj} * f_h\left(\sum_{i=1}^{n}\left(w_{j,i} + x_i\right) + b_j\right)\right\} + b_k\right] \quad (1)$$

Where $\hat{y}_K$= output variable, x_i=input variable, n = number of neurons in the input layer (number of input variables), m =number of neurons in hidden layer, $w_{j,i}$=the weights of input hidden layer, w_{kj}= weights hidden output layers, b_j= bias of the hid-den layer, b_k=bias of the output layer, f_h= activation function of the hidden layer, f_o= activation function of the output layer [18][18].

The effectiveness of an ANN model is influenced by the architecture of the ANN; the training algorithm and the mathematical functions. The second function is the training phase where the optimum value of weights determined by minimizing an error function. Hyperbolic tangent was the activation function between the input and hidden layers while identity was the activation functions between the hidden and output layers. The online type of training was selected which updates the synaptic weights after every single training data record, while to avoid overtraining, maximum training epochs computed automatically, and to specify the optimization algorithm, the gradient descent method was selected. When the difference between the output and target values, E, is larger than an acceptable value then the values of the weights and bias are readjusted using “gradient descent” method in which the change in weights Δw_{kj} is expressed in the form:

$$\Delta w_{kj} = -\alpha \frac{\partial E}{\partial w_{kj}} \tag{2}$$

where α =learning rate. High values of α result in high changes in weights w_{jk} during each iteration. This can result in the predicted value not converging to the most optimum combination of values. Small values of α yield small changes in weights w_{kj}, and small values of Δw_{kj} for each iteration. Although more training time is required, the iterative process results in more accurate ANN predictions.

4.2. Adopted ANN models

The developed ANN models in this study were used to predict the axial compressive strength and strain for CFPT specimens tested under the concentric load. Since the confined stress and strain of concrete have been expressed as a function of lateral confinement pressure in several existing stress-strain models, the latter was computed for the CFPT specimens and the values were summarized in Table 2. Four ANN models were developed; two models to predict the axial compressive strength and strain of unconfined concrete, ANN-I and ANN-II, and the remaining two, ANN-III and ANN-IV, for predicting the axial compressive strength and the strain of CFPT. For ANN-I and ANN-II models, 36 test data for unconfined concrete were used for training and testing. A similar number of experimental results were used for training and testing of ANN-III and ANN-IV models for CFPT.

The data used in ANN models were arranged in a format of three input parameters that included the water-cement ratio, aggregate cement ratio, and slump in addition to the bias. Each ANN model has four neurons (nodes) in the input layer and one neuron in the output layer as demonstrated in Fig. 2 for ANN-III. One hidden layer was selected with six neurons for strain models, while for strength models the number was seven neurons, was determined due to its minimum absolute percentage error values for training and testing sets. The input-hidden layer weights (wj,i) and the hidden-output layer weights (wk,j) yield high flexibility to adapt to the data freely. The models use different parameters to evaluate their influences on the ability of the subject models to yield accurate predictions. When only compressive strength was considered as an input parameter, the ANN model was found to predict the elastic modulus of concrete well within the ranges of the input parameters considered [19].

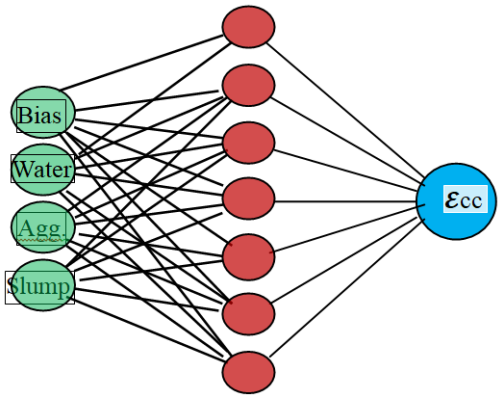

Fig. 2. Architecture of ANN-IV Model, strain at peak stress.

Table 2
Test results for unconfined concrete and CFPT specimens.

Specimens	$f'co$ (MPa)	$f'cc$ *Exp*	$f'cc / f'co$ *Exp EX*	$f'cc$ *ANN*	$f'cc / f'co$ *ANN*	$fl/f'co$ *Exp*	ε_{co}	ε_{cc} *Exp*
CT-A1	38.7	47.21	1.22	47.31	1.24	0.0714	0.00197	0.0112
CT-A2	38.7	48.38	1.25	47.31	1.24	0.0714	0.0019	0.0113
CT-A3	38.7	47.6	1.23	47.31	1.24	0.0714	0.00192	0.011
CT-B1	37.2	46.13	1.24	47.08	1.26	0.0742	0.00187	0.010
CT-B2	37.2	46.5	1.25	47.08	1.26	0.0742	0.00188	0.0125
CT-B3	37.2	47.62	1.28	47.08	1.26	0.0742	0.0018	0.0112
CT-C1	34.7	44.76	1.29	45.46	1.29	0.0796	0.00179	0.0096
CT-C2	34.7	44.42	1.28	45.46	1.29	0.0796	0.00188	0.0089
CT-C3	34.7	45.8	1.32	45.46	1.29	0.0796	0.00182	0.0099
CT-D1	32.9	41.45	1.26	44.38	1.34	0.0840	0.00177	0.0082
CT-D2	32.9	45.73	1.39	44.38	1.34	0.0840	0.00173	0.0083
CT-D3	32.9	44.42	1.35	44.38	1.34	0.0840	0.00179	0.009
CT-E1	32.2	44.11	1.37	43.59	1.38	0.0858	0.00168	0.0081
CT-E2	32.2	45.08	1.4	43.59	1.38	0.0858	0.00176	0.0086
CT-E3	32.2	44.76	1.39	43.59	1.38	0.0858	0.00169	0.0081
CT-F1	31.2	42.43	1.36	43.12	1.4	0.0885	0.00172	0.0077
CT-F2	31.2	43.99	1.41	43.12	1.4	0.0885	0.00174	0.0079
CT-F3	31.2	44.62	1.43	43.12	1.4	0.0885	0.00171	0.008
CT-G1	28.6	40.04	1.4	39.79	1.39	0.0966	0.00169	0.0071
CT-G2	28.6	40.9	1.43	39.79	1.39	0.0966	0.00176	0.0078
CT-G3	28.6	40.46	1.415	39.79	1.39	0.0966	0.00169	0.0076
CT-H4	25.5	37.74	1.48	37.36	1.47	0.1083	0.00157	0.007
CT-H5	25.5	38.51	1.51	37.36	1.47	0.1083	0.00172	0.0073
CT-H6	25.5	36.98	1.45	37.36	1.47	0.1083	0.00182	0.0071
CT-I1	20.4	31.42	1.54	33.33	1.56	0.1354	0.00164	0.0067
CT-I2	20.4	32.44	1.59	33.33	1.56	0.1354	0.00165	0.0068
CT-I3	20.4	32.03	1.57	33.33	1.56	0.1354	0.00165	0.007
CT-J1	19.2	31.49	1.64	30.71	1.67	0.1439	0.00169	0.0061
CT-J2	19.2	31.49	1.64	30.71	1.67	0.1439	0.00151	0.0064
CT-J3	19.2	32.45	1.69	30.71	1.67	0.1439	0.00158	0.0067
CT-K1	16.7	29.39	1.76	29.7	1.76	0.1654	0.00153	0.0055
CT-K2	16.7	29.89	1.79	29.7	1.76	0.1654	0.00154	0.0059
CT-K3	16.7	29.22	1.75	29.7	1.76	0.1654	0.00169	0.0052
CT-L1	16.3	30.32	1.86	29.89	1.83	0.1695	0.00153	0.0052
CT-L2	16.3	29.99	1.84	29.89	1.83	0.1695	0.00164	0.005
CT-L3	16.3	29.67	1.82	29.89	1.83	0.1695	0.00167	0.0051

5. Statistical indexes

In the current study five different statistical indexes were used for assessing the performance of the trained ANN models and the performance of several existing FRP-confined concrete strength and strain models. The indexes included: Average absolute relative error (AAE), Normalized root-mean-square error (NRMSE), Nash–Sutcliffe efficiency (E), Modified Nash–Sutcliffe efficiency (E1), and coefficient of correlation (R^2), Table 3. Where the model prediction is expressed by (model.i), the experimental value is represented by (exp.i), and N is the total number of data. Lower AAE's and NRMSE indicate good model performance. While an E value in excess of 0.80 is considered good. The Modified Nash–Sutcliffe efficiency (E1) is based on absolute deviations instead of squares of the deviations. The R^2 expresses the rate of association between the two variables and many outliers result in weak R^2. Since most values of RMSE are smaller than those of AAE, the former is easier to use.

Table 3
Statistical indexes for evaluating the performances of the models.

Statistical indexes	Mathematical expression
Average absolute relative error (AAE)	$AAE = \frac{\sum_{i=1}^{N} \left\lvert \frac{model.i - exp.i}{exp.i} \right\rvert}{N}$
Normalized root-mean-square error (NRMSE)	$NRMSE = \frac{\sqrt{\frac{\sum_{i=1}^{N}(exp.i - model.i)^2}{N}}}{\sum_{i=1}^{N} exp.i}$
Nash–Sutcliffe efficiency (E)	$E = 1 - \frac{\sum_{i=1}^{N}(exp.i - model.i)^2}{\sum_{i=1}^{N}(exp.i - aver.exp.i)^2}$
Modified Nash–Sutcliffe efficiency (E1)	$E1 = 1 - \frac{\sum\lvert exp.i - model.i\rvert}{\sum\lvert exp.i - aver.exp.i\rvert}$
Coefficient of correlation (R^2)	$R^2 = \left(\frac{\sum_{i=1}^{N}(exp.i - exp.i\ aver)\ (model.i - model.i\ aver)}{\sum_{i=1}^{N}(exp.i - exp.i\ aver)^2\ \sum_{i=1}^{N}(model.i - model.i\ aver)^2} \right)^2$

6. Results and discussions

6.1. Compressive strength

The correlation between the experimental strength of CFPT and unconfined concrete strength was shown in Fig. 3, with R^2=0.636. When the same figure was plotted using the ANN predicted values for CFPT only, the value of R^2 improved slightly to 0.647, Fig. 4. When ANN-1 was used for modeling strength of unconfined concrete (fco) very good correlation was observed between the ANN predicted strength and the corresponding experimental values, Fig. 5, with the value of the coefficient of the determination being equal to 0.995. The strength prediction of the ANN-III model for CFPT specimens (fcc_{ANN}) was plotted in Figs. 6 versus the experimental strength (fcc_{Exp}) with a good correlation. As it is depicted in Figs. 7 the values for compressive strength of CFPT obtained from the training and testing in ANN-III model were in good agreement with

experimental results. An artificial neural network is a regression model having the ability to predict the output of the non-linear input in a precise manner [20]. The trained neural network was able to reproduce the experimental test results.

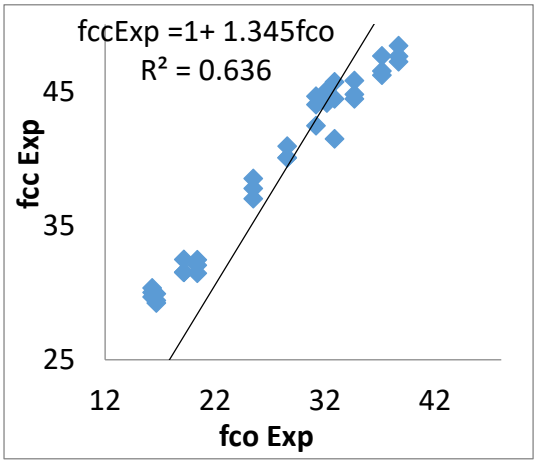

Fig. 3. Strength of CFPT (fcc_{Exp}) versus strength of concrete (fco_{Exp}).

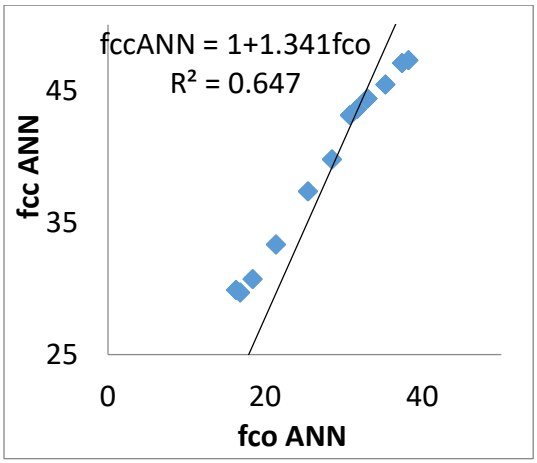

Fig. 4. Relationship between predicted strength of CFPT (fcc_{ANN}) and concrete (fco_{Exp}).

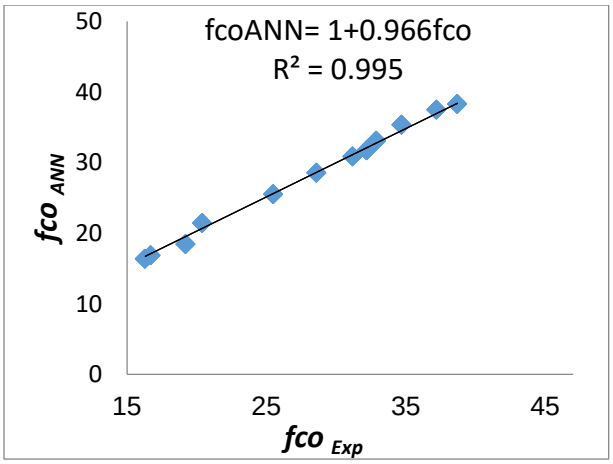

Fig. 5. Predicted fco_{ANN} versus experimental strength of concrete fco_{Exp}.

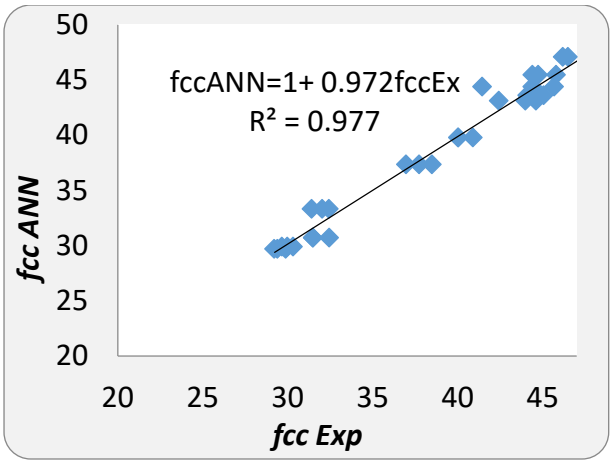

Fig. 6. Predicted fcc_{ANN} versus experimental strength fcc_{Exp} of CFPT.

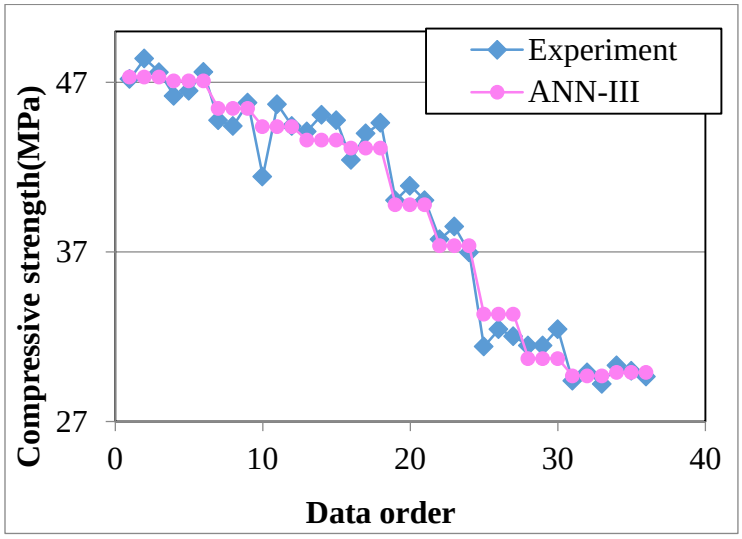

Fig. 7. Comparison of predicted-experimental compressive strength.

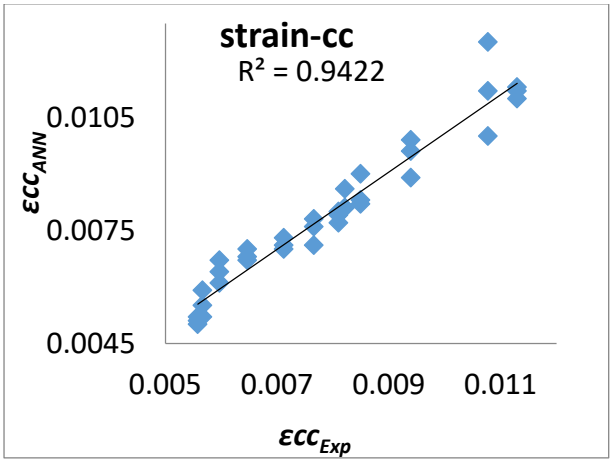

Fig. 8. Predicted-experimental strain of CFPT.

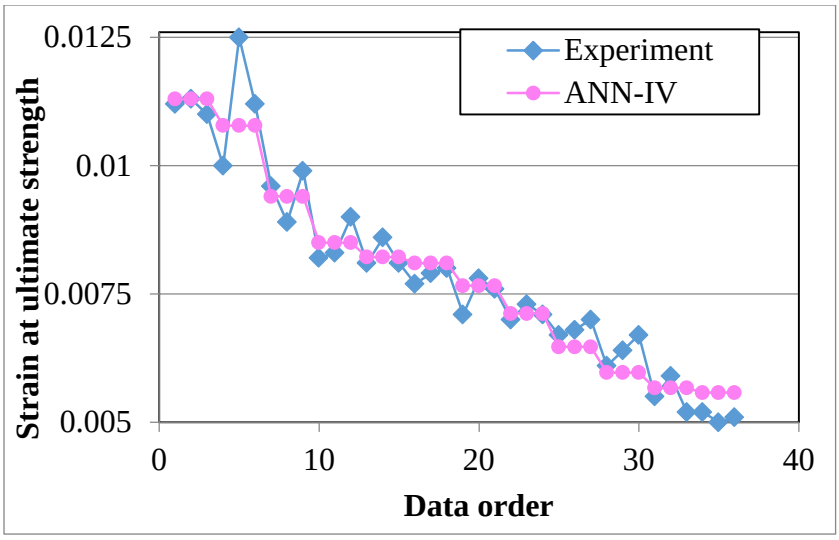

Fig. 9. Comparison of predicted-experimental strain at ultimate strength of CFPT.

6.2. Strain at ultimate strength

The correlation between predicted strain at ultimate strength (ε_{ccANN}) and its corresponding experimental (ε_{ccExp}) values for CFPT were plotted in Fig. 8 with an R^2 value equal to 0.942. The difference between the predicted and the experimental values for the strain at ultimate strength was depicted in Fig. 9. The adopted ANN model was capable of deriving the relationship of input variables and the output.

6.3. Compressive strength-strain relationship

A linear correlation was observed between the experimental compressive strength and the strain, Fig. 10 with a reasonable coefficient of correlation R^2= 0.794. Using predictions from the two ANN models for CFPT, the correlation between the two parameters changed by 11% from R^2= 0.794 to R^2= 0.881, Fig. 11. The experimental strength enhancement ratio (*fcc/fco*) versus confinement ratio (*fl/fco*) was plotted in Fig.12. The strength enhancement ratio, calculated from the ratio of the strength of CFPT to strength of the corresponding specimen without plastic tube, was increased due to the use of the plastic tube. The confinement ratio (*fl/fco*) was calculated from the following:

$$\left[\frac{f_l}{f_{co}}\right]_P = \frac{2t_P}{D_i}\frac{\varepsilon_P E_P}{f_{co}} = \frac{2t_P}{D_i}\frac{f_{y,P}}{f_{co}} \quad (3)$$

Where t_P=thickness of plastic tube; ε_P =ultimate tensile strain; E_P= the modulus of elasticity of tube; $f_{y,P}$ =yield strength of tube; D_i =internal diameter of tube; f_l =lateral confinement pressure [2]. Based on regression analysis of experimental results, the following expression for the strength of CFPT was obtained:

$$\left(\frac{f_{cc}}{f_{uc}}\right)_{Exp} = 1 + 3.068\left(\frac{f_l}{f_{co}}\right) \quad (4)$$

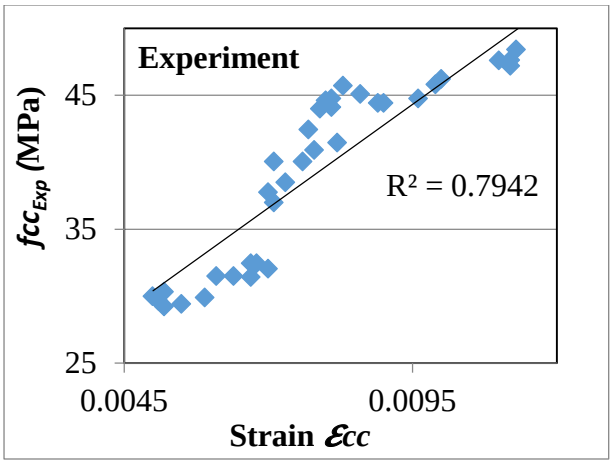

Fig. 10. Relationship between compressive strength-strain of CFPT.

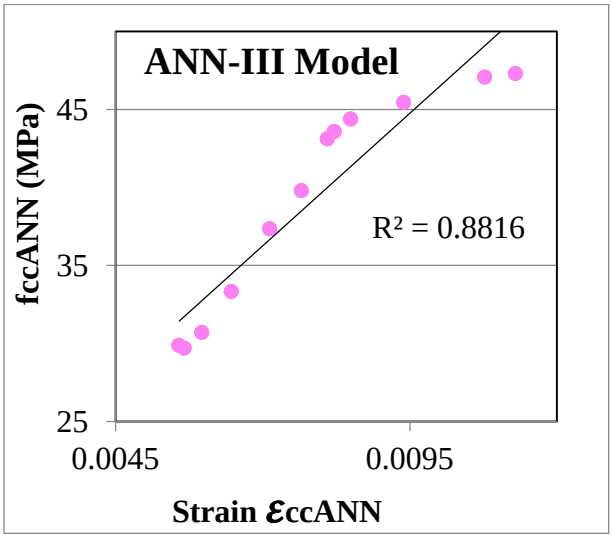

Fig. 11. Relationship between predicted peak stress and predicted strain at peak stress of CFPT.

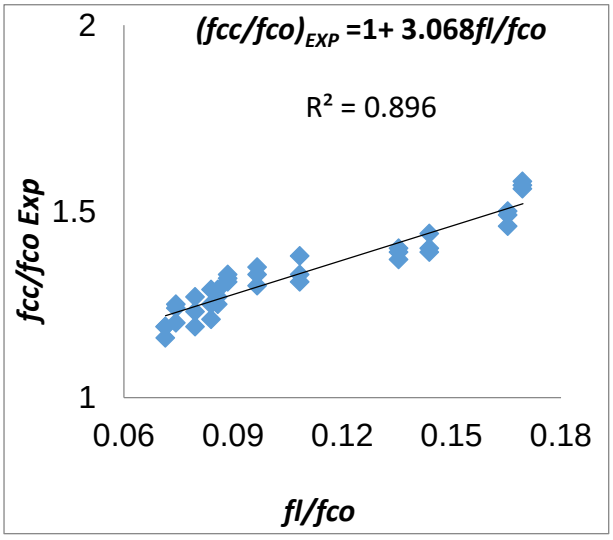

Fig. 12. Experimental strength enhancement ratio versus confinement ratio (*fl/fco*).

The predicted fcc_{ANN}/fco ratio versus (fl/fco) was depicted in Fig. 13. A second expression for the strength of CFPT was obtained from Fig. 13 as follows:

$$\left(\frac{f_{cc}}{f_{uc}}\right)_{ANN} = 1 + 4.39\left(\frac{f_l}{f_{co}}\right) \quad (5)$$

The coefficient of correlation for Eq. (5), R2=0.935, was better than for Eq. (4) with R^2=0.896, Fig. 12. The experimental strain ratio ($\varepsilon cc_{Exp}/\varepsilon_{co}$)-confinement ratio ($fl/fco$) relationship was presented in Fig. 14, while the predicted strain ratio ($\varepsilon cc_{ANN}/\varepsilon_{co}$)-confinement ratio ($fl/fco$) relationship was shown in Fig. 15. In both Figures the relationship was modeled by a function which is a nonlinear combination of the model parameters.

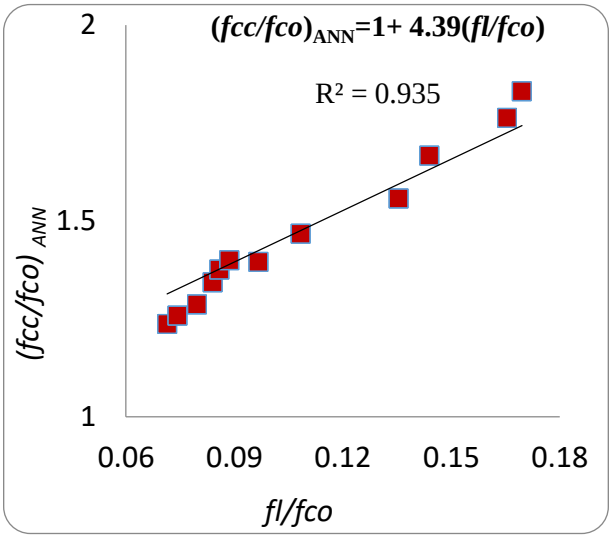

Fig. 13. Predicted strength enhancement ratio (ANN) versus confinement ratio (fl/fco).

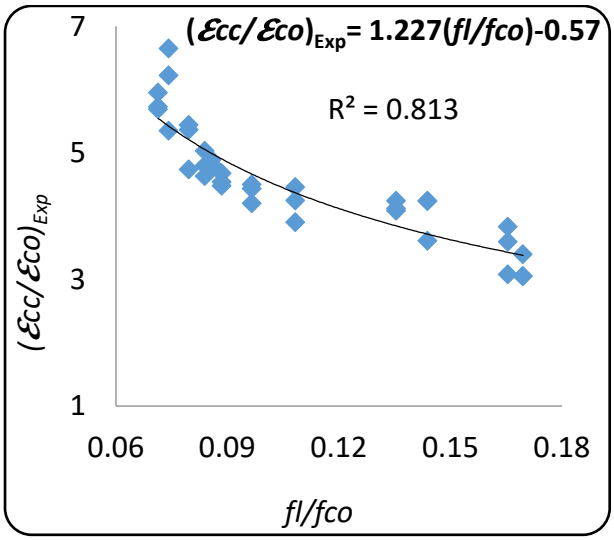

Fig. 14. Experimental strain ratio $\varepsilon_{cc}/\varepsilon_{co}$ versus confinement ratio (fl/fco).

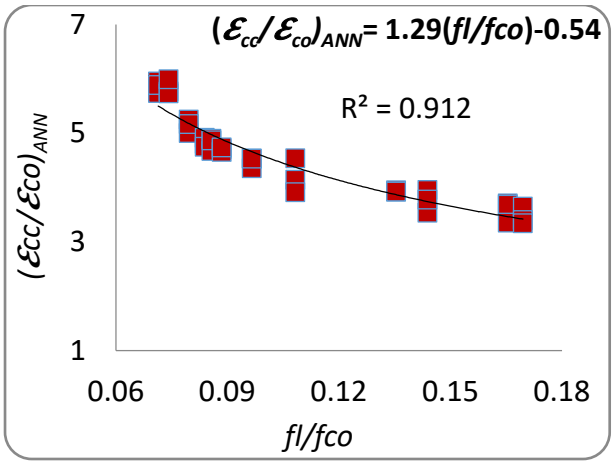

Fig. 15. Predicted strain ratio $(\varepsilon_{cc}/\varepsilon_{co})_{ANN}$ versus confinement ratio (*fl/fco*).

The following two equations were obtained for determining strain of CFPT based on regression analysis of experimental and ANN predicted values, respectively:

$$\left(\frac{\varepsilon_{cu}}{\varepsilon_{co}}\right)_{Exp} = 1.277\left(\frac{f_l}{f_{co}}\right)^{-0.57} \tag{6}$$

$$\left(\frac{\varepsilon_{cu}}{\varepsilon_{co}}\right)_{ANN} = 1.29\left(\frac{f_l}{f_{co}}\right)^{-0.54} \tag{7}$$

The negative sign indicated the decrease in strain with increase in confinement ratio. The experimental results for strain at ultimate strength were more sporadic than the corresponding values for compressive strength. Another two equations for determining $(\varepsilon_{cc}/\varepsilon_{co})$ ratio were obtained using the strength enhancement ratio as the variable parameter:

$$\left(\frac{\varepsilon_{cu}}{\varepsilon_{co}}\right)_{Exp} = 8.097\left(\frac{fcc}{f_{co}}\right)^{-02.87} \tag{8}$$

$$\left(\frac{\varepsilon_{cu}}{\varepsilon_{co}}\right)_{ANN} = 7.298\left(\frac{fcc}{f_{co}}\right)^{-1.3} \tag{9}$$

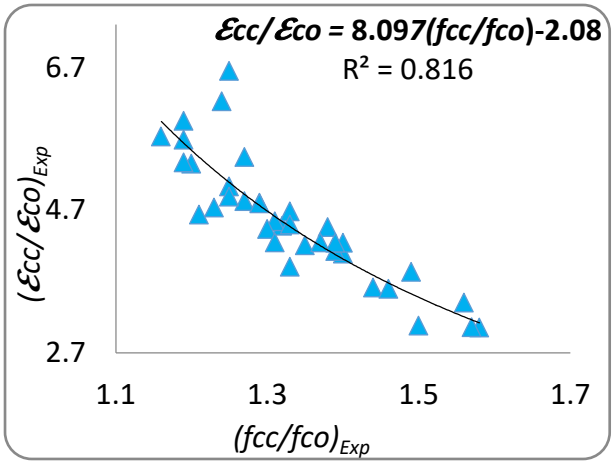

Fig. 16. Experimental strain ratio $(\varepsilon_{cc}/\varepsilon_{co})_{Exp}$ versus strength ratio (*fcc/fco*).

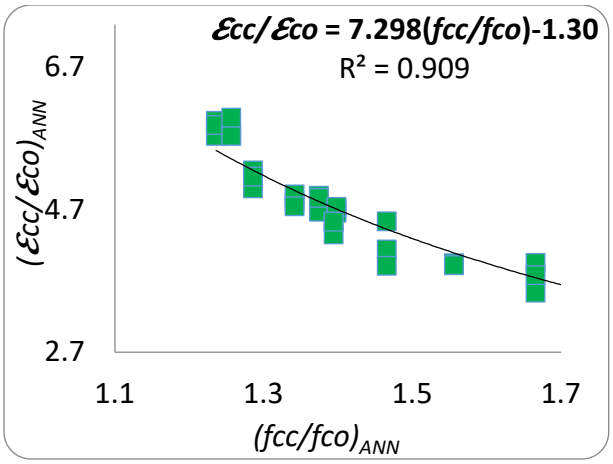

Fig. 17. Predicted strain ratio $(\varepsilon_{cc}/\varepsilon_{co})_{Exp}$ versus strength ratio (*fcc/fco*).

Using ANN modeling predictions result in an improved correlation where value of R^2 increased from 0.816 to 0.909, as is shown in Figs. 16 and 17 for experimental and predicted values of (*fcc/fco*), respectively.

6.4. FRP-confined concrete models

Based on the experimental results, the ANN predictions were compared with predictions from existing six FRP-confined concrete strength equations [21–26], Table 4. All the ratios of predicted strength $(fcc/fco)_{Pre}$ to the experimental strength $(fcc/fco)_{Exp}$ were computed in Table 5. Five statistical indexes and several other statistical measures such as standard deviations and coefficient of variance, Table 5, were used to compare the performance of the strength models. The strength model which was considered to yield the best predictions was that displaying the lowest values of AAE and RSME and the highest value of R^2. The mean error for the FRP models in predicting the experimental results were 50.5%, 7.406%, 34.4%, 17.6%, 12.91%, and 7.45%, while for Eqs. (4) and (5) were 8.84% and 2.80%, respectively.

Table 4
Strength models for FRP-confined concrete.

Source	Model
Mirmiran [21]	$\frac{f_{cc}}{f_{co}} = 1 + 4.269\left(\frac{f_{lu}}{f_{co}}\right)^{0.587}$
Guralnick and Gunawan [22]	$\frac{f_{cc}}{f_{uc}} = 1 + 2.2\left(\frac{f_{lu}}{f_{co}}\right)^{0.828}$
Yan and Pantelides [23]	$\frac{f_{cc}}{f_{co}} = 0.0768\ln\left(\frac{f_{lu}}{f_{co}}\right) + 1.122$
Binici [24]	$\frac{f_{cc}}{f_{co}} = 1.8\left(\frac{f_{lu}}{f_{co}}\right)^{0.3}$ If $\left(\frac{f_{lu}}{f_{co}}\right) < 0.14$
Wu and Wang [25]	$\frac{f_{cc}}{f_{co}} = 1 + 2.23\left(\frac{f_{lu}}{f_{co}}\right)^{0.96}$
Wu et al. [26]	$\frac{f_{cc}}{f_{uc}} = 0.75 + 2.5\left(\frac{f_{lu}}{f_{co}}\right)$

Table 5
Predicted/ experimental ratios of *(fcc/fco)* using FRP and proposed ANN models.

Specimen	*fcc/fco Exp*	$(fcc/fco)_{Pre}/(fcc/fco)_{Exp}$							
		[21]	[22]	[23]	[24]	[25]	[26]	Eq.(4)	Eq.(5) ANN
CT-A1	1.22	1.59	1.01	0.74364	0.913	0.95	0.99	1.214	1.08
CT-A2	1.25	1.55	1.01	0.74364	0.913	0.92	0.99	1.214	1.05
CT-A3	1.23	1.58	1.01	0.74364	0.913	0.94	0.99	1.214	1.07
CT-B1	1.24	1.59	1	0.73368	0.902	0.94	0.98	1.223	1.07
CT-B2	1.25	1.58	1	0.73368	0.902	0.93	0.98	1.223	1.06
CT-B3	1.28	1.54	1	0.73368	0.902	0.91	0.98	1.223	1.04
CT-C1	1.29	1.56	0.99	0.72117	0.889	0.91	0.98	1.239	1.05
CT-C2	1.28	1.57	0.99	0.72117	0.889	0.92	0.98	1.239	1.05
CT-C3	1.32	1.52	0.99	0.72117	0.889	0.89	0.98	1.239	1.02
CT-D1	1.26	1.62	0.96	0.69432	0.858	0.94	0.95	1.252	1.09
CT-D2	1.39	1.47	0.96	0.69432	0.858	0.85	0.95	1.252	0.98
CT-D3	1.35	1.51	0.96	0.69432	0.858	0.87	0.95	1.252	1.01
CT-E1	1.37	1.5	0.94	0.67881	0.84	0.86	0.93	1.257	1
CT-E2	1.4	1.47	0.94	0.67881	0.84	0.84	0.93	1.257	0.98
CT-E3	1.39	1.48	0.94	0.67881	0.84	0.85	0.93	1.257	0.99
CT-F1	1.36	1.52	0.93	0.66911	0.829	0.88	0.92	1.266	1.02
CT-F2	1.41	1.47	0.93	0.66911	0.829	0.84	0.92	1.266	0.99
CT-F3	1.43	1.45	0.93	0.66911	0.829	0.83	0.92	1.266	0.97
CT-G1	1.4	1.52	0.94	0.67581	0.842	0.86	0.94	1.29	1.02
CT-G2	1.43	1.49	0.94	0.67581	0.842	0.84	0.94	1.29	1
CT-G3	1.4	1.51	0.94	0.67581	0.842	0.85	0.94	1.29	1.02
CT-H1	1.48	1.49	0.92	0.64883	0.815	0.83	0.92	1.325	1
CT-H2	1.51	1.46	0.92	0.64883	0.815	0.82	0.92	1.325	0.98
CT-H3	1.45	1.52	0.92	0.64883	0.815	0.85	0.92	1.325	1.02
CT-I1	1.54	1.55	0.91	0.62212	0.799	0.84	0.92	1.406	1.04
CT-I2	1.59	1.5	0.91	0.62212	0.799	0.81	0.92	1.406	1
CT-I3	1.57	1.52	0.91	0.62212	0.799	0.82	0.92	1.406	1.02
CT-J1	1.64	1.48	0.87	0.58401	0.756	0.8	0.88	1.432	1
CT-J2	1.64	1.48	0.87	0.58401	0.756	0.8	0.88	1.432	1
CT-J3	1.69	1.44	0.87	0.58401	0.756	0.78	0.88	1.432	0.97
CT-K1	1.76	1.45	0.85	0.55818	0.736	0.77	0.87	1.496	0.98
CT-K2	1.79	1.42	0.85	0.55818	0.736	0.76	0.87	1.496	0.96
CT-K3	1.75	1.46	0.85	0.55818	0.736	0.77	0.87	1.496	0.99
CT-L1	1.86	1.38	0.82	0.53853	0.713	0.73	0.84	1.509	0.94
CT-L2	1.84	1.4	0.82	0.53853	0.713	0.74	0.84	1.509	0.95
CT-L3	1.82	1.41	0.82	0.53853	0.713	0.75	0.84	1.509	0.96
Minimum		1.382	0.823	0.539	0.71307	0.733	0.843	0.824	0.938
Maximum		1.618	1.009	0.744	0.9129	0.946	0.994	0.982	1.086
Average		1.501	0.927	0.656	0.82423	0.847	0.926	0.911	1.009
COV		0.003	0.003	0.004	0.00377	0.004	0.002	0.002	0.001
STD		0.057	0.057	0.065	0.06184	0.06	0.045	0.047	0.037
AAE%		50.5	7.406	34.4	17.6	12.91	7.45	8.8	2.80
NRMSE		0.014	0.003	0.01	0.005	0.004	0.003	0.003	9E-04
E		0.726	0.989	0.869	0.962	0.978	0.991	0.988	0.997
E1		0.491	0.917	0.64	0.813	0.86	0.919	0.9035	0.972
R^2		0.976	0.978	0.97	0.979	0.979	0.979	0.979	0.979

The corresponding values of NRMSE were 0.014, 0.003, 0.01, 0.005, 0.004, 0.003 for FRP models and 0.003, and 9E-04 for the Eqs. (4) and (5), respectively. The E and E1 values for the FRP models in predicting the experimental results were 0.726, 0.898, 0.869, 0.962, 0.991 and 0.491, 0.917, 0.64, 0.813, 0.86, 0.919, respectively, while for Eqs. (4) and (5) were 0.988, 0.997, and 0.903, 0.972, respectively. The results for the minimum, maximum, average, STD and COV values were also given in Table 5. The FRP models obtained by linear and non-linear regression analysis were not able to predict the strength of CFPT with high accuracy. The observed divergence between the predictions and the experimental test values was highest for the strength model given in [21]. The statistical analysis indicated the inability of the strength model expressed by Eq. (4) to yield a close fit to the test data similar to that of the ANN technique. The statistical values in Table 5 showed that the proposed ANN model expressed by Eq. (5) was more suitable and can better predict the strength of CFPT.

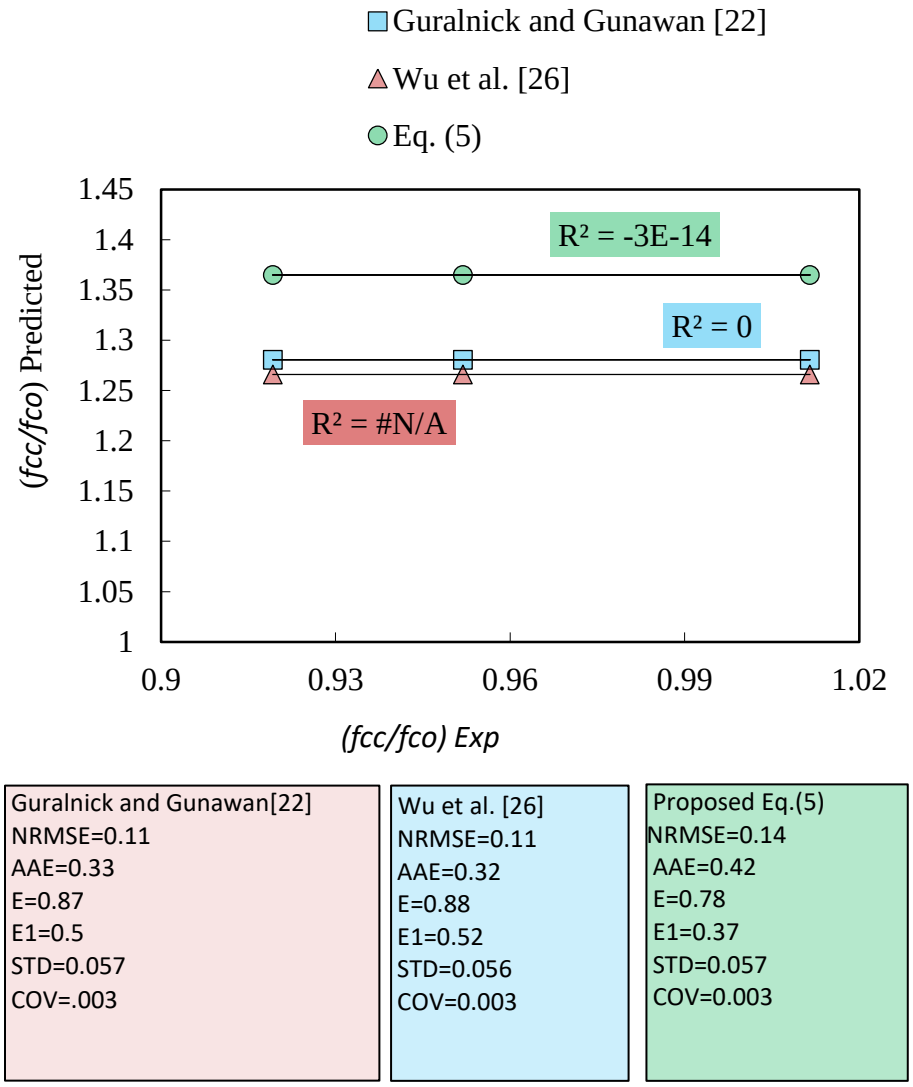

Fig. 18. Predicted versus experimental strength enhancement ratio (*fcc/fco*) using data from [27].

6.5. Performance of strength models

In order to indicate the accuracy of the ANN strength model predictions, the CFPT experimental strength results for the *fc/fco* ratio reported by Fakharifar and Chen [27] were selected; 1.011, 0.952, and 0.919 with fco= 49.5MPa. The experimental results were compared to the strength predictions from ANN and two best performing FRP models, Table 5. As is illustrated in Fig. 18, the ANN prediction yielded acceptable values. Although the mean error value 42% for the ANN model predictions was slightly higher than for the other two models, 33 and 32%. The main cause of such error was the lack of enough data in the present study for the training of the ANN model for higher strengths.

6.6. Predicted/Experimental strain ratios

The predicted values of strain ratio $(\varepsilon_{cc}/\varepsilon_{co})_{Pre}$ using the six FRP-confined concrete strain models [26,28–32] and the developed Eq. (7), Table 6, were plotted versus experimental $(\varepsilon_{cc}/\varepsilon_{co})_{Exp}$ values in Fig. 19. The developed model yielded a better agreement between the predicted and experimental results, where most of the data points lie in the ratio range of 4 to 6 in Fig. 19. Predictions by models in [30] and [32] lie in the same range ratio, too. However, the statistical indexes for the latter two models are much higher. The accuracy of the proposed model was checked and the AAE values were 52.5, 75.05, 23.9, 35.9, 77.23, and 29.8 for FRP models [26,28–32] respectively, while it was 6.58 for Eq. (7). Other statistical measures that show the trends of model performance were presented in Table 7. Based on the Eq. (7), the soft computing method yielded the predictions with the best correlation with the test data. This performance indicates that the ANN models were capable of generalizing between input and output parameters with sufficiently closed data.

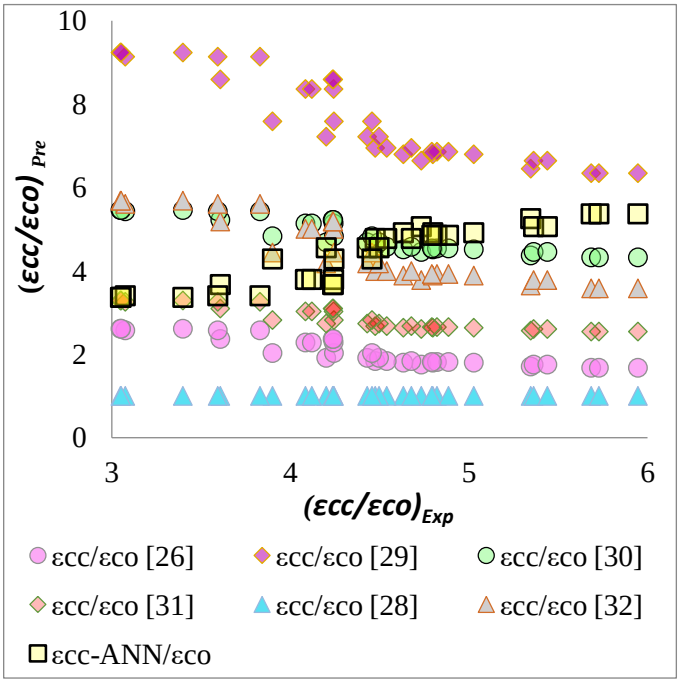

Fig. 19. Predicted versus experimental strain ratio (fcc/fco) using FRP-confined concrete and proposed strain models.

Table 6
Strain models for FRP-confined concrete.

Source	Model
Wu et al. [26]	$\frac{\varepsilon_{cu}}{\varepsilon_{co}} = 1.3 + 6.3\left(\frac{f_{lu}}{f_{co}}\right)$
Karbhari and Gao [28]	$\frac{\varepsilon_{cu}}{\varepsilon_{co}} = 1 + 0.01\left(\frac{f_{lu}}{f_{co}}\right)$
Ilki et al [29]	$\frac{\varepsilon_{cu}}{\varepsilon_{co}} = 1 + 20\left(\frac{f_{lu}}{f_{co}}\right)^{0.5}$
Al-Tersawy et al. [30]	$\frac{\varepsilon_{cu}}{\varepsilon_{uc}} = 1 + 8.16\left(\frac{f_{lu}}{f_{uc}}\right)^{0.34}$
Mohamed H, Masmoudi [31]	$\frac{\varepsilon_{cu}}{\varepsilon_{co}} = 2 + 7.6\left(\frac{f_{lu}}{f_{co}}\right)$
Sadeghian and Fam [32]	$\frac{\varepsilon_{cu}}{\varepsilon_{co}} = 1 + 15.93\left(\frac{f_{lu}}{f_{co}}\right)^{0.69}$

Table 7
Statistics of predicted/experimental ratios of $(\varepsilon_{cc}/\varepsilon_{co})_{Pre}/(\varepsilon_{cc}/\varepsilon_{co})_{Exp}$ using FRP and proposed ANN models.

Model	$(\varepsilon_{cc}/\varepsilon_{co})_{Pre}/(\varepsilon_{cc}/\varepsilon_{co})_{Exp}$						
	[26]	[28]	[29]	[30]	[31]	[32]	Eq.(7) ANN
Minimum	0.256546981	0.386	0.1505	0.97	0.657	0.5366	0.79
Maximum	0.856311568	1.079	0.3286	3.029	1.792	1.8219	1.107
Average	0.474933956	0.653	0.2277	1.749	1.106	1.0875	0.983
COV	0.028356502	0.035	0.0019	0.326	0.092	0.122	0.006
STD	0.169575614	0.188	0.0444	0.575	0.306	0.3517	0.08
AAE%	52.5	77.23	75.05	23.9	35.9	29.8	6.58
NRMSE	0.0169	0.01245	0.02229	0.02109	0.00853	0.00937	0.00248
E	0.6489	0.8064	0.3856	0.4328	0.9212	0.889	0.9666
E1	0.43	0.601	0.1974	0.33	0.776	0.7079	0.931
R^2	0.741	0.741	0.741	0.761	0.767	0.753	0.797

7. Conclusions

The application of artificial neural networks to predict the strength of CFPT was examined in this study using 72 test data. The input variables of the study included outer diameter, water/cement ratio, slump, aggregate/cement ratio, and compressive strength of unconfined concrete. The following conclusions can be drawn:

1. The tests carried out in this study illustrate the feasibility of using ANN to predict the compressive strength and strain at ultimate strength of CFPT stub columns. The ANN model, which was built, trained, and tested using the experimental test results, yielded predictions close

to the experimental results. With proper training, ANN can give an alternative procedure for predicting the strength of CFPT.

2. Based on Artificial Neural Networks, a new model was proposed for predicting the compressive strength of uPVC-confined concrete stub columns tested under axial compression loading.

3. The performance of the proposed ANN model was assessed by comparing the strength predictions with predictions from several existing FRP strength models. Comparison of NRMSE values using the FRP and the proposed models showed the lowest NRMSE value was for the ANN model predictions. Additionally, the ANN model predictions had the highest correlation coefficient (R^2), and the lowest AAE value. The ANN procedure displays strong potential as a viable technique for predicting the strength of CFPT within the range of input parameters considered.

4. It was observed that the values of strain at ultimate strength based on the ANN model predictions were more precise than those computed from several empirical equations on the basis of the test results.

The ANN model seems promising for evaluating the compressive strength and strain at ultimate strength of CFPT specimens. With its generalization capability it can be applied to other studies to predict the strength of stub CFPT columns.

Funding

This research received no external funding.

Conflicts of interest

The authors declare no conflict of interest.

References

[1] Wang J-Y, Yang Q-B. Investigation on compressive behaviors of thermoplastic pipe confined concrete. Constr Build Mater 2012;35:578–85.

[2] Abdulla NA. Influence of plastic pour-in form on mechanical behavior of concrete. Structures 2019;19:193–202. doi:10.1016/j.istruc.2019.01.007.

[3] Abdulla NA. Concrete filled PVC tube: A review. Constr Build Mater 2017;156:321–9. doi:10.1016/j.conbuildmat.2017.08.156.

[4] Kamal A. Multi-layer UPVC piping system. QScience Proc 2016;2016:30. doi:10.5339/qproc.2016.qgbc.30.

[5] Ahmad A, Kotsovou G, Cotsovos DM, Lagaros ND. Assessing the accuracy of RC design code predictions through the use of artificial neural networks. Int J Adv Struct Eng 2018;10:349–65. doi:10.1007/s40091-018-0202-4.

[6] Noorzaei J, Hakim SJS, Jaafar MS, Thanoon WAM. Development of artificial neural networks for predicting concrete compressive strength. Int J Eng Technol 2007;4:141–53.

[7] Hakim SJS, Noorzaei J, Jaafar MS, Jameel M, Mohammadhassani M. Application of artificial neural networks to predict compressive strength of high strength concrete. Int J Phys Sci 2011;6:975–81.

[8] Prasad BKR, Eskandari H, Reddy BVV. Prediction of compressive strength of SCC and HPC with high volume fly ash using ANN. Constr Build Mater 2009;23:117–28.

[9] Uysal M, Tanyildizi H. Estimation of compressive strength of self compacting concrete containing polypropylene fiber and mineral additives exposed to high temperature using artificial neural network. Constr Build Mater 2012;27:404–14. doi:10.1016/j.conbuildmat.2011.07.028.

[10] Kasperkiewicz J, Racz J, Dubrawski A. HPC Strength Prediction Using Artificial Neural Network. J Comput Civ Eng 1995;9:279–84. doi:10.1061/(ASCE)0887-3801(1995)9:4(279).

[11] Jahangir H, Esfahani MR. Numerical Study of Bond – Slip Mechanism in Advanced Externally Bonded Strengthening Composites. KSCE J Civ Eng 2018;22:4509–18. doi:10.1007/s12205-018-1662-6.

[12] Naderpour H, Kheyroddin A, Amiri GG. Prediction of FRP-confined compressive strength of concrete using artificial neural networks. Compos Struct 2010;92:2817–29. doi:10.1016/j.compstruct.2010.04.008.

[13] Abdulla NA. Mechanical Behavior of Slender Composite Columns under Axial Compression Load. KSCE J Civ Eng 2020;24:208–18. doi:10.1007/s12205-020-0669-y.

[14] Woldemariam AM, Oyawa WO, Nyomboi T. Reliability assessment of axially loaded uPVC tube confined reinforced concrete columns. Structures 2020;23:529–38. doi:10.1016/j.istruc.2019.11.009.

[15] Saadoon AS, Jasim NA. Prediction of Ultimate Strength of PVC-Concrete Composite Columns Using FIS Models 2017.

[16] Abdulla NA. Concrete Encased with Engineering Plastics. J Civ Eng Constr 2020;9:31–41. doi:10.32732/jcec.2020.9.1.31.

[17] Tasdemir MA, Tasdemir C, Akyüz S, Jefferson AD, Lydon FD, Barr BIG. Evaluation of strains at peak stresses in concrete: A three-phase composite model approach. Cem Concr Compos 1998;20:301–18. doi:10.1016/S0958-9465(98)00012-2.

[18] Dreyfus G. Neural networks: methodology and applications. Springer Science & Business Media; 2005.

[19] Demir F. Prediction of elastic modulus of normal and high strength concrete by artificial neural networks. Constr Build Mater 2008;22:1428–35. doi:10.1016/j.conbuildmat.2007.04.004.

[20] Dutta RK, Rao TG, Sharma A. Application of Random Forest Regression in the Prediction of Ultimate Bearing Capacity of Strip Footing Resting on Dense Sand Overlying Loose Sand Deposit. J Soft Comput Civ Eng 2019;3:28–40.

[21] Mirmiran A. Analytical and experimental investigation of reinforced concrete columns encased in fiberglass tubular jacket and use of fiber jacket for pile splicing. 1997.

[22] Guralnick SA, Gunawan L. Strengthening of Reinforced Concrete Bridge Columns with FRP Wrap. Pract Period Struct Des Constr 2006;11:218–28. doi:10.1061/(ASCE)1084-0680(2006)11:4(218).

[23] Yan Z, Pantelides CP. Design-oriented model for concrete columns confined with bonded FRP jackets or post-tensioned FRP shells. Proc. 8th Int. Symp. Fiber Reinf. Polym. Reinf. Concr. Struct., University of Patras; 2007.

[24] Binici B. Design of FRPs in circular bridge column retrofits for ductility enhancement. Eng Struct 2008;30:766–76. doi:10.1016/j.engstruct.2007.05.012.

[25] Wu Y-F, Wang L-M. Unified Strength Model for Square and Circular Concrete Columns Confined by External Jacket. J Struct Eng 2009;135:253–61. doi:10.1061/(ASCE)0733-9445(2009)135:3(253).

[26] Wu H-L, Wang Y-F, Yu L, Li X-R. Experimental and Computational Studies on High-Strength Concrete Circular Columns Confined by Aramid Fiber-Reinforced Polymer Sheets. J Compos Constr 2009;13:125–34. doi:10.1061/(ASCE)1090-0268(2009)13:2(125).

[27] Fakharifar M, Chen G. Compressive behavior of FRP-confined concrete-filled PVC tubular columns. Compos Struct 2016;141:91–109. doi:10.1016/j.compstruct.2016.01.004.

[28] Karbhari VM, Gao Y. Composite Jacketed Concrete under Uniaxial Compression—Verification of Simple Design Equations. J Mater Civ Eng 1997;9:185–93. doi:10.1061/(ASCE)0899-1561(1997)9:4(185).

[29] Ilki A, Kumbasar N, Koc V. Low strength concrete members externally confined with FRP sheets. Struct Eng Mech 2004;18:167–94.

[30] Al-Tersawy SH, Hodhod OA, Hefnawy AA. Reliability and code calibration of RC short columns confined with CFRP wraps. Proceedings, eighth Int. Symp. fiber Reinf. Polym. Reinf. Concr. Struct., 2007, p. 122–30.

[31] Mohamed HM, Masmoudi R. Axial Load Capacity of Concrete-Filled FRP Tube Columns: Experimental versus Theoretical Predictions. J Compos Constr 2010;14:231–43. doi:10.1061/(ASCE)CC.1943-5614.0000066.

[32] Sadeghian P, Fam A. Improved design-oriented confinement models for FRP-wrapped concrete cylinders based on statistical analyses. Eng Struct 2015;87:162–82. doi:10.1016/j.engstruct.2015.01.024.